Experimental Investigation of the In-Cylinder Tumble Motion inside GDI Cylinder at Different Planes under Steady-State Condition using Stereoscopic-PIV

Mohammed El-Adawy[1][†], M. R. Heikal[1, 2] and A. Rashid A. Aziz[1]

[1]*Mechanical Engineering Department, University Technology PETRONAS, Perak, Seri Iskandar, 32610,
Centre for Automotive Research and Electric Mobility (CAREM)*
[2]*University of Brighton, Brighton BN2 4GJ, UK*

†*Corresponding Author Email: engmohammed_2008@yahoo.com*

ABSTRACT

This paper describes an experimental study aimed at the characterization of the steady-state tumble motion in the cylinder of an engine using stereoscopic particle image velocimetry (Stereo-PIV). More specifically, a pent-roof four valves gasoline direct injection (GDI) engine head was mounted on a modified FEV steady-state flow rig for applying Stereo-PIV at different measurement vertical tumble planes at mid cylinder, mid injector and mid valve. The flow field was described by the distribution of the ensemble average flow patterns for 1000 pairs of images for every case, vorticity contours, turbulent kinetic energy and tumble ratio. The results revealed that the higher velocities acquired at the mid valve plane improved the turbulent kinetic energy and tumble ratio compared to the other planes. There was a good level of agreement between direct and indirect methods used for calculating the tumble ratio.

Keywords: Tumble motion; Stereo PIV; Flow bench; Tumble ratio; GDI engine.

NOMENCLATURE

B	Bore	TKE	Turbulent kinetic energy
m	Number of vectors in x-axis	TR	Tumble ratio
n	Number of vectors in y-axis	VL	Valve lift
PIV	Particle image velocimetry	x_c, y_c	Co-ordinates of the center of field of view
RMS	Root mean square	ω	Angular speed
S	Stroke	ΔP	Pressure difference across the intake valves

1. INTRODUCTION

During the last century, internal combustion engines (ICE) have been widely developed by the automotive industry for powering light and heavy-duty vehicles. Even though engine design and technology have improved considerably, research is still continuing as the issues of air pollution and market competitiveness have become increasingly important. With the recent regulations and standards for exhaust emissions and fuel consumption there is, more than ever, the need for an accurate control of the in-cylinder combustion process Korakianitis *et al.*(2011), Wallner *et al*. (2008), Baratta *et al*. (2015). It is generally accepted that the large-scale flow structures created during the induction stroke have a significant influence on the mixing process and the combustion behavior of the engine. Traditionally, swirl has been used to reduce cyclic variability and produce faster burn rates both in compression and spark ignited engines. However, tumble has been introduced as an alternative to swirl for enhancing the cyclic stability in homogeneous charge engines Heywood *et al.* (1988), Kim *et al*. (2006), Zhang *et al*. (2014), Fu *et al*. (2016), Baratta *et al*. (2017). Tumble Ports are now a standard means of controlling the combustion process in modern engines. The large-scale tumbling motion is generally created during the intake stroke by restricting the flow rate on the outer side of the inlet valve using straight ports oriented in such a way that most of the annular jet exiting the valve is directed towards the exhaust side Buhl *et al*. (2017), Payri *et al.* (2004), Falfari *et al*. (2014). In addition, the

tumble motion is enhanced greatly by using valve masking techniques but to the detriment of the engine breathing demand at high speeds or high loads Millo *et al*. (2014). Shrouded valves are, nevertheless, unattractive solutions for production engines due to the weight increase and the fact that rotation must be prevented.

Two different methods can be used to assess the in-cylinder tumble motion: macroscopic (direct) and microscopic (indirect) approaches. The macroscopic methods evaluate the in-cylinder motion using some integral parameters such as flow coefficient, discharge coefficient, swirl ratio and tumble ratio…etc., where steady-state flow rigs are considered as one of these methods. On the other hand, the microscopic methods can provide more details about the in-cylinder flow behavior. These methods include optical engines along with laser diagnostics such as laser Doppler anemometry (LDA) Shuliang *et al.* (2000) and particle image velocimetry (PIV) Li *et al*. (2003), Liu *et al*. (2012), Begg *et al*. (2009), Muller *et al*. (2010), Wang *et al*. (2011). Whilst, the other type of microscopic methods is the Computational Fluid Dynamics (CFD) simulation.

It is worth recalling that the target tumble ratios are usually evaluated during the early stages of engine design Kim *et al*. (2006). Subsequently, an accurate quantification of the tumble motion behavior for a certain engine head layout is considered as a significant factor in the process of engine design. As a matter of fact, the steady state flow testing is considered as the most widely adopted procedure for tumble motion quantification Baratta *et al*. (2017), Lee et al. (2007). In the automotive industry, steady-state flow rigs are standard and economical ways of characterizing the in-cylinder gas motion. They have been traditionally used to deter-mine the integral flow parameters such as tumble ratio, flow coefficient, discharge coefficient, gulp factor…. etc. El-Adawy *et al*. (2017) (a), M. El Adawy *et al*. (2017) (b). With the advent of more sophisticated mixture flow strategies in engines to meet the re-cent pollution standard, the understanding of in-cylinder flow characteristics became more than ever a challenge for the research community. Therefore, there is a pressing need to obtain more detailed information on the flow characteristics such as turbulence structures, turbulent kinetic energy, turbulent intensity…etc., as these parameters have significant effects on the mixing process.

Traditional mechanical techniques for obtaining this detailed information can give time or space averaged descriptions of the in-cylinder flow behavior, whereas laser techniques can provide data with high time and space resolutions. Among these laser techniques, particle image velocimetry (PIV) is a well-established and popular non-intrusive optical measurement technique that is capable of providing whole field instantaneous velocity measurements simultaneously Reuss *et al*. (1988). Previous PIV measurements in IC engines have characterized turbulence properties Reuss *et al*. (2000), analyzed spatial flow structure Funk *et al*. (2002), investigated influences of cycle-to-cycle variations Voisine *et al.*

(2011), as well as characterized flows during injection and ignition Druault *et al*. (2005). Recently, Stereoscopic high-speed time-resolved particle image velocimetry (Stereo-PIV) can be used to go further in the investigation of the in-cylinder flow behavior. Therefore, it is expected that the combination of the modified steady-state flow rig (macroscopic) and the high speed stereoscopic time-resolved PIV technique (microscopic) can be considered as a first step towards deeper understanding of the flow characteristics El-Adawy *et al. (2018)*. Moreover, the steady-state flow rig can allow these studies independent of the interaction of the piston geometry and simplifies the problem by eliminating the dynamic effects and cycle to cycle variations of the running engines and thus provides a better understanding of the physical parameters influencing the flow characteristics.

In this experimental study, stereo-PIV was applied to GDI engine head, with the objective of investigating the in-cylinder tumble flow evolution during the intake stroke under steady-state conditions in three different vertical tumble-planes, i.e. parallel to the cylinder axis. These planes included the mid-cylinder plane (plane of symmetry), the mid-injector plane and the mid-intake valve plane. The planes were selected to provide the best insight into the in-cylinder flow behavior and to gain a reasonable estimation of the tumble ratio under steady-state conditions. The data were selected during the in-take stroke for fixed values of valve lifts namely; 7 mm, 8 mm, 9 mm and 10 mm and a fixed pressure drop (ΔP) of 150 mmH$_2$O across the air intake valves.

2. EXPERIMENTAL SET UP

The experimental set up can be divided into two basic components: the steady-state flow bench and the stereo-PIV system.

2.1 Steady-State Flow Bench

The FEV steady-state flow bench shown in Fig. 1 used a centrifugal compressor to create the air flow into the cylinder. The rig operated in intake mode (suction) inducting the air through the intake port, intake valves, the cylinder and a rotary piston gas flow meter. A pent-roof four-valves GDI cylinder head was used as shown in Fig. 2. The two intake valves were adjusted using a micrometer and positioned at constant valve lifts 7 mm, 8 mm, 9 mm and 10 mm. The measurements were carried out at a constant pressure difference of 150 mmH$_2$O across the air intake valves. The pressure adjustment required for different valve lift settings was achieved by a by-pass valve controlled by a stepper motor. A transparent cylinder liner was made of Plexiglas having an internal bore diameter of 92.5mm, length ('stroke') of 116 mm and wall thickness of 3 mm.

2.2 Stereoscopic PIV

The experimental set-up of stereo PIV consisted of a pulsed laser system, two CCD-cameras, two stereo (Scheimpflug) camera mounts, calibration target and advanced software for data processing. The stereo-PIV measurements were carried out in the vertical
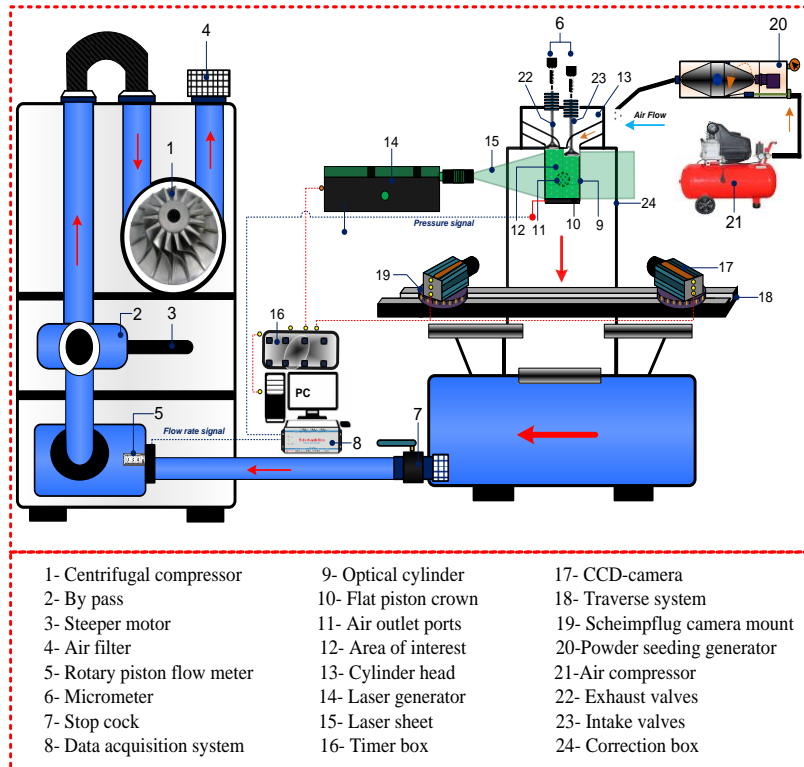
1- Centrifugal compressor	9- Optical cylinder	17- CCD-camera
2- By pass	10- Flat piston crown	18- Traverse system
3- Steeper motor	11- Air outlet ports	19- Scheimpflug camera mount
4- Air filter	12- Area of interest	20-Powder seeding generator
5- Rotary piston flow meter	13- Cylinder head	21-Air compressor
6- Micrometer	14- Laser generator	22- Exhaust valves
7- Stop cock	15- Laser sheet	23- Intake valves
8- Data acquisition system	16- Timer box	24- Correction box

Fig. 1. Schematic of Stereo-PIV set up on the steady-state flow bench.

tumble plane (z=0) which was parallel to the cylinder axis and parallel to a line joining the inlet and exhaust valves. Additional Stereo-PIV measurement planes were investigated at the mid-inlet valve plane (z = 20 mm 'toward the camera'), and the mid injector plane situated on one side of the mid-cylinder plane position (z=8mm), as shown in Fig 3.
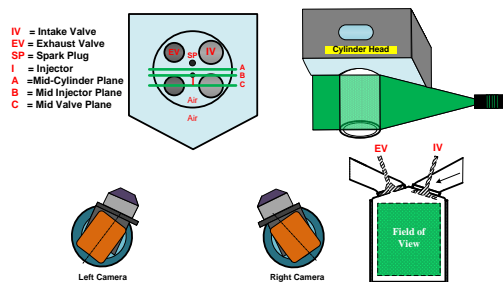

Fig. 2. Spray-guided GDI cylinder head.

Fig. 3. Top view for the location of the measurement vertical tumble planes.

Fig. 1 shows a schematic diagram of the experimental setup of the time-resolved stereoscopic PIV system. The in-cylinder air flow was seeded with Titanium Dioxide (TiO_2) solid particles using a solid powder seeder. The flow field was illuminated twice using LDY 303 PIV Nd: YLF double pulsed laser capable of 20 mJ at 1 kHz at 527nm per laser head per pulse. The displacement of seeding particles was captured using a pair of Speed Sense M310 Dantec Dynamics CCD high speed cameras running in double frame mode from different viewing angles. For every valve lift, 1000 pairs of images (1280 pixels by 800 pixels, 12-bit grey scale) were acquired and saved directly to the hard drive of the computer for analysis. The Scheimpflug principle was fulfilled when the best focus over the entire image, for each camera.

2.2.1 Image Processing

The PIV processing was accomplished by utilizing DANTEC Dynamics Studio software which included three stages: pre-processing, vector calculation and post-processing. The pre-processing stage denoted also as "raw image processing stage "is an important stage to enhance the quality of the raw images and increases the signal to noise ratio (SNR) of data. This is because the raw images were affected by several noise sources such as, multiple reflections of particles, background light and extra laser reflections due to the effect of curved surfaces. Therefore, background subtraction and masking out of the unwanted regions were employed as pre-processing techniques to eliminate these issues. The evaluation was carried out using adaptive correlation techniques with a size of 32×32 pixels interrogation

area and 50% overlapping. The post-processing of the resulting velocity vector maps was carried out using two validation techniques to fix and repair the spurious vectors: The moving average validation and the average filter. PIV measurements depend on detecting seeding particles motion to calculate the flow velocity. Random error and bias (systematic) error are the main sources of uncertainty in digital PIV measurements Coleman *et al (2009).* Gaining a velocity vector field with minimal uncertainty relies on number of parameters such as, seeding particles, optical medium, camera configuration (setting), PIV algorithm (interrogation area, post processing... etc.). The Uncertainty of PIV measurements for the current study was estimated using the particle disparity approach in the Dynamic Studio software Sciacchitano *et al.* (2013). The particle disparity technique identifies individual particles on frame 1 & 2 and tries to match pairs based on the measured displacement vectors. Using this technique, the error in the magnitude of velocities was lower than 3 %. More details about the stereoscopic PIV processing can be found in El-Adawy et al. (2018-b)

4. RESULTS AND DISCUSSTIONS

4.1 Spatial Flow Structures

Averages of 1000 PIV instantaneous vector maps were produced at different positions including the mid-cylinder plane A (z=0), the mid injector plane B (z=8 mm), and the mid-intake valve plane C (z=20 mm). Fig. 4 shows the ensemble average velocity vector fields of the in-cylinder tumble motion at the different measurement planes for fixed values of valve lift 7 mm, 8 mm, 9 mm and 10 mm. A number of observations were extracted from this figure. Firstly, although the differences between the three planes were clearly visible in the vector maps, some similarities could be found in the flow patterns. In all measurement and for all valve lifts, a significant amount of the incoming air flow was directed towards the exhaust side in the form of a jet-like structure. Because of the interaction between this jet flow and the left cylinder wall then the flat piston at the bottom of the cylinder, a strong tumble vortex was generated in the counter clock wise direction. The intensity of this vortex increased with increasing the valve lift. In addition, this vortex was more significant especially at valve lift 10 mm as it dominated the full cylinder with no dramatic change in the flow pattern could really be noticed between the different positions and represented an ideal solid body rotation model. Secondly, one of the more significant observations from these contour plots was the differences in flow structures between the mid injector and the mid cylinder planes, and the mid valve plane where the presence of the intake valve caused a separate vortex to form under the intake valve. Thirdly, the average flow velocity was higher in the mid valve plane for all cases. The average velocity increased from 7.5 m/s to 7.96 m/s and from 12.1 m/s to 12.7 for valve lifts 8 mm and 10 mm respectively when comparing between mid-cylinder and mid valve
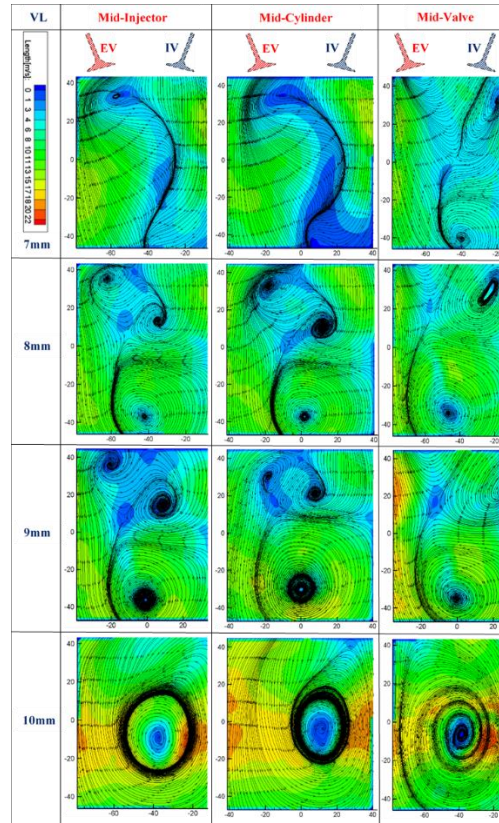

Fig. 4. Ensemble average velocity vector fields at different measurement tumble planes.

planes. Fourthly, the fact that the position of the vortex center in the tumble planes did not change dramatically across the cylinder volume for all valve lifts, indicated a potentiality of the tumble pattern to remain during the compression stroke. Moreover, the measurements indicated that while the dominant tumble vortex was mostly two dimensional, other flow structures confirm that there were other significant three dimensional features of the flow which must be considered when evaluating air/fuel mixing in the cylinder.

4.2 Vorticity Contours

Vorticity is a very important quantity for characterizing turbulence and its rotational structures. Vorticity is defined by the curl of the velocity vector. For a three dimensional vector field the vorticity is defined by:

$$curl\ V = \nabla \times V = \xi = \left(\frac{\partial v_z}{\partial y} - \frac{\partial v_y}{\partial z}\right)\vec{i} + \left(\frac{\partial v_x}{\partial z} - \frac{\partial v_z}{\partial x}\right)\vec{j} + \left(\frac{\partial v_y}{\partial z} - \frac{\partial v_x}{\partial y}\right)\vec{k} \quad (1)$$

Where V is the velocity vector and $\vec{i}$, $\vec{j}$ and $\vec{k}$ are the unit vectors in *X*, *Y* and *Z* axis.

PIV provides the instantaneous velocity fields from which the curl of the vector field which is equivalent to the vorticity can be calculated from the velocity gradients. The spatial average of the velocity magnitude was extracted from 1000 velocity vector fields using Dynamic-Studio software, as shown in the equation below:

$$\xi = \left(\frac{\partial v}{\partial x} - \frac{\partial u}{\partial y}\right) \quad (2)$$

Fig. 5 illustrated the vorticity maps in the different measurement planes for different valve lifts. It can be noticed that the vorticity magnitudes were positive and negative indicating the different direction of vortices' spins seen in the velocity vector maps. The figure clearly shows the strength of vorticity increased in both directions of rotation with increasing the valve lift except for valve lift 10 mm which was dominated by a strong counter clock wise tumble vortex with a center coinciding with the center of the cylinder. Moreover, when comparing for the same valve lift at different planes, it was found that there were not significant changes in the vortex strength and shape except for the mid valve plane which was distinguished with reverse tumble vortex behind the intake. This is might be attributed to the fact that, for a single valve with straight perpendicular port exiting into a finite volume, the inducted steady-state flow streamlines form a torus, as some of the fluid particles come back to the axis of symmetry of the valve. However, in real engines, the vortex can be dramatically distorted by the boundaries of the confined space defined by the cylinder walls and pent roof surfaces. As the air jet impinges onto these boundaries, the flow is directed and, in some cases, heavily restricted. For design consideration, the inlet valve is rarely centered in the cylinder, thus uneven angular distribution of the flow rate around the valve is significant. Therefore, for the current study, the flow was highly restricted on the right side of the intake valves (the effect of the restriction decrease with increasing the valve lift), thus a reverse tumble vortex was formed behind the intake valves because of the interaction between the right air jet with internal boundaries of the cylinder head and cylinder.
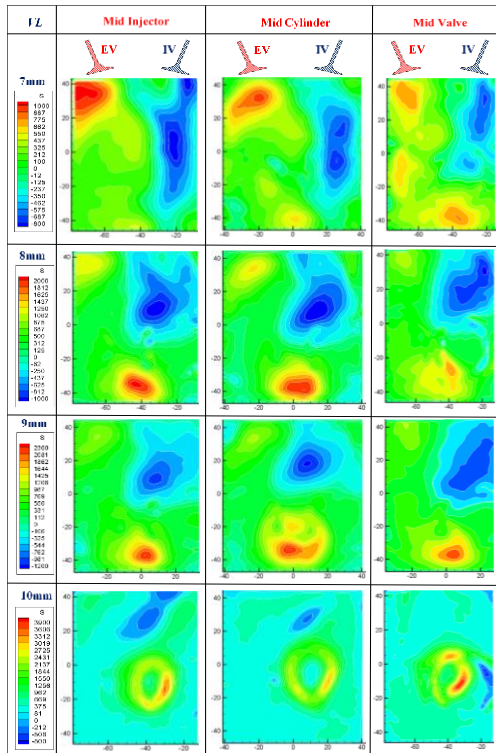

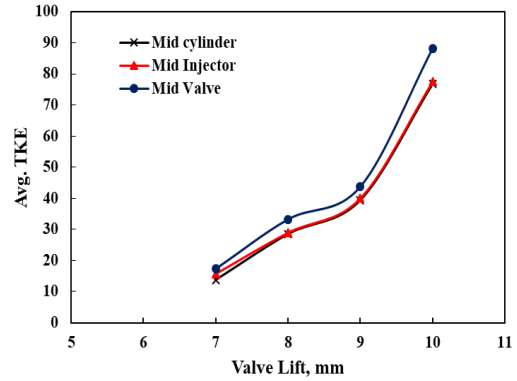**Fig. 5. Vorticity maps at different measurement tumble planes.**

Fig. 6. Avg. TKE at different measurement tumble planes.

Moreover, for the mid valve plane, it can be noticed that with increasing the valve lift the strength of the reverse tumble vortex behind the intake valve decrease while on the other hand the main large scale tumble motion developed until it dominated the whole cylinder at valve lift 10 mm for all measurement planes.

In addition, one method of studying the increase in vortex strength was to observe the turbulent kinetic energy of the flow field at different planes.

3.3 Average Turbulence Kinetic Energy (TKE)

In the world of fluid dynamics, turbulence plays a significant contribution in the mixing mechanisms as the velocity fluctuations enhance mixing and turbulence dispersion. The kinetic energy provides quantitative information for the better understanding of turbulence mechanisms since it is affiliated with both fluctuating and mean velocities. The turbulence kinetic energy (TKE) is that part of the kinetic energy of the fluid that exists in the fluctuation velocities and was calculated using a mathematical expression given by Reuss Reuss *et al.* (2000). It was calculated from the root mean square (RMS) velocity vector fields, which were obtained from ensemble average velocity fields by Dynamic-Studio V5 software which in-turn were obtained from 1000 instantaneous velocity vector fields.

$$TKE = \frac{1}{2}\rho V_{rms}^2 = \frac{1}{2}\rho(u_{rms}^2 + v_{rms}^2 + w_{rms}^2) \quad (3)$$

Where 'u_{rms}', 'v_{rms}' and 'w_{rms}' are the RMS velocity components in the X, Y and Z directions respectively, and 'ρ' is the air density

The intensity of the turbulent mixing in the different measurement planes for different valve lifts can be expressed by the TKE as shown in Fig. 6. As expected, increasing the valve lift led to higher flow rates inside the cylinder with high mean and fluctuating velocities which in-turn enhanced the TKE and increased the strength of the air motion Krishna *et al.* (2016). Agarwal *et al.* (2018) also reported similar behavior of TKE in the intake stroke using an optical engine. The lower intensity of the TKE at valve lift 7 mm could be attributed to the collision between the intake jet-side with the exhaust jet-side. Moreover, the TKE was

higher for the mid valve plane for all valve lifts which agreed well with the higher velocities acquired in this plane. This practically means that the intake generated vortices in all planes at high valve lifts could persist through the compression stroke.

3.4 Tumble Ratio

Two different methods were used to calculate the tumble ratio in the different planes. The first method was based on angular momentum (TR$_1$) while the second method was based on vorticity (TR$_2$). TR$_1$ was defined by the ratio of the actual angular momentum of the fluid to the total fluid mass M assuming solid body motion at crank angle speed ω while the center of rotation was taken to be the center of the field of view Stansfield *et al.* (2007).

$$TR_1(x_c, y_c) = 8.\frac{\sum_{i=1}^{m}\sum_{j=1}^{n}(v_{ij} \cdot (x_c - x_{i,j}) - (u_{ij} \cdot (y_c - y_{i,j}))}{(m.n).\omega.B^2}$$

(4)

ω is the angular speed of the crank shaft (rad/sec) which was estimated based on constant axial velocity across the bore in the steady port flow bench condition defined as Druault *et al.* (2005):

$$\omega = \frac{4\dot{m}}{B^2.S.\rho_{cyl}}$$

(5)

TR$_2$ was defined as the mean value of vorticity normalized by twice the crank angle speed ω. The mean vorticity was calculated by considering the rotation of horizontal and vertical velocity components about the center of field of view as follows Huang *et al.* (2005):

$$TR_2 = \frac{\sum_{i=1}^{m}\sum_{j=1}^{n}\xi_{i,j}}{2.(m.n).\omega} = \frac{\sum_{i=1}^{m}\sum_{j=1}^{n}\left(\frac{\partial v}{\partial x} - \frac{\partial u}{\partial y}\right)}{2.(m.n).\omega}$$
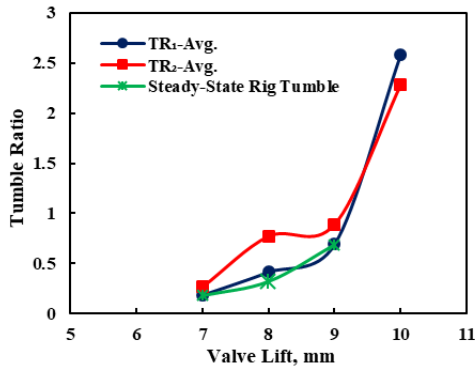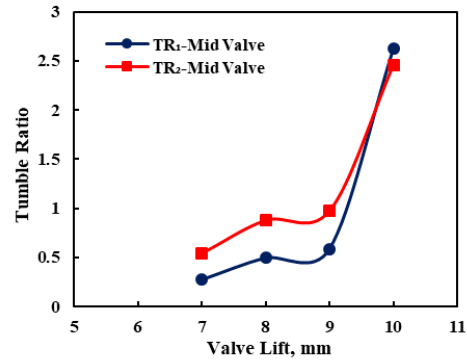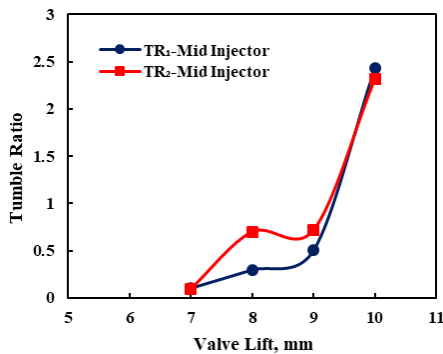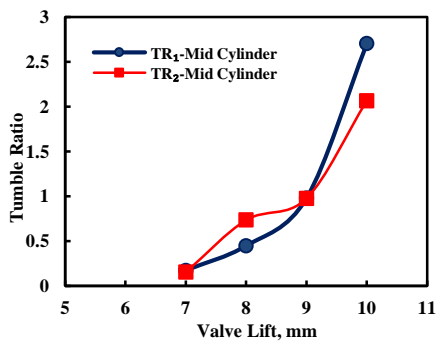
(6)

Fig. 7. Tumble ratios calculated from both the curl of the vector field and the angular velocity at different measurement planes.

This ratio represents the relative amounts of large and small scale rotation in the flow. For a rotating solid body, the mean vorticity has a constant value of twice the angular velocity. Fig. 7 shows the tumble ratio calculated from both the angular momentum and from the curl of the vector fields. It is clear from the figure that both methods showed the same trend namely, the tumble ratio magnitude increased with increasing the valve lift indicating an improvement in overall in-cylinder air motion. It can be noticed that the high values of tumble ratio for all planes especially at high valve lift (10mm) generated an outstandingly good tumble pattern as the vortex occupies the entire cylinder volume and high velocities were generated. Nevertheless, the lower values of tumble ratio generated for valve lift 7mm could be attributed to the fact that at this valve lift the tumble vortex started to form especially at the mid valve plane which had higher values of tumble ratio compared to the other planes. While the lower values of tumble ratio for valve lifts 8 and 9 mm could be attributed to the two counter rotating vortices generated because of the interaction between the jets coming from both sides of the intake valve. A counter rotating vortex had an impact on the flow pattern as it prevented the main vortex from filling the complete cylinder volume and affected the stability of the tumble pattern. In addition, the tumble level was gained by assessing the rotational speed of the paddle wheel anemometer to calculate the non-dimensional rig-tumble, for more details see El-Adawy *et al.* (2017) (a). It can be seen that; the trend of non-

dimensional rig-tumble values was the same as the average values of tumble ratio for different planes. The difference between both curves might be related to the fact that for PIV, the values were calculated for a certain number of vertical planes in two dimensions. However, the paddle wheel result was an 'integral' of the three dimensional flow structures. Furthermore, the calculation was carried out on the ensemble average values of all the velocity vector fields at each valve lift and measurement plane. Table 1 gives a summary of the tumble ratios calculated form both the curl of the vector field and the angular velocity at different measurement tumble planes side by side with the non-dimensional tumble rig measured on the steady-state rig-tumble (the paddle wheel rotation).

5. CONCLUSIONS

The FEV steady-state flow rig was modified for applying stereoscopic particle image velocimetry in different measurement tumble planes; mid cylinder, mid injector, and mid valve at different valve lifts. The in-cylinder flow was characterized using parameters which included the ensemble average of the velocity field, vorticity contours, TKE and tumble ratio. The following conclusions were drawn:

- The fact that the location of the vortex center in the tumble planes did not vary greatly across the cylinder volume at high valve lifts indicated a uniform overall three-dimensional shape of the tumbling pattern.

Table 1 Tumble ratios calculated from PIV measurements and paddle wheel rotation

ΔP [mmH$_2$O]	Measurement Plane	Valve Lift [mm]	PIV Tumble Ratio	
			TR$_1$	TR$_2$
150	Mid Cylinder	7	0.173	0.154
	Mid Injector		0.103	0.098
	Mid Valve		0.274	0.540
	Average for Planes		0.183	0.264
	Rig Tumble		0.179	
	Mid Cylinder	8	0.447	0.735
	Mid Injector		0.298	0.702
	Mid Valve		0.496	0.878
	Average for Planes		0.413	0.771
	Rig Tumble		0.320	
	Mid Cylinder	9	0.979	0.976
	Mid Injector		0.503	0.721
	Mid Valve		0.588	0.975
	Average for Planes		0.69	0.890
	Rig Tumble		0.688	
	Mid Cylinder	10	2.70	2.06
	Mid Injector		2.43	2.32
	Mid Valve		2.62	2.46
	Average for Planes		2.58	2.28
	Rig Tumble		—	

- A far more effective tumble pattern was observed with higher velocity magnitudes and flow structures closer to solid body rotation at valve lift 10 mm for all tumble positions.

- The higher velocities generated at the mid valve plane improved the overall air motion inside the cylinder in terms of higher TKE and tumble ratios compared to the other planes

- There was a good level of agreement between direct (integral) and indirect (calculated from the measured velocity field) methods used for calculating the tumble ratio.

ACKNOWLEDGEMENT

REFERENCES

Agarwal, A. K., S. Gadekar and A. P. Singh (2018). In-Cylinder Flow Evolution Using Tomographic Particle Imaging Velocimetry in an Internal Combustion Engine. *Journal of Energy Resources Technology* 140(1), 012207.

Baratta, M. and D. Misul (2015). Development of a method for the estimation of the behavior of a CNG engine over the NEDC cycle and its application to quantify for the effect of hydrogen addition to methane operations. *Fuel* 140, 237-249.

Baratta, M., D. Misul, E. Spessa, L. Viglione, G. Carpegna and F. Perna (2017). Experimental and numerical approaches for the quantification of tumble intensity in high-performance SI engines. *Energy Conversion and Management* 138, 435-451.

Begg, S. M., M. P. Hindle, T. Cowell and M. R. Heikal (2009). Low intake valve lift in a port fuel-injected engine. *Energy* 34(12), 2042-2050.

Buhl, S., F. Gleiss, M. Köhler, F. Hartmann, D. Messig, C. Brücker and C. Hasse (2017). A combined numerical and experimental study of the 3D tumble structure and piston boundary layer development during the intake stroke of a gasoline engine. *Flow, Turbulence and Combustion* 98(2), 579-600.

Coleman, H. W. and W. G. Steele (2009). Experimentation, validation, and uncertainty analysis for engineers.

Druault, P., P. Guibert and F. Alizon (2005). Use of proper orthogonal decomposition for time interpolation from PIV data. *Experiments in Fluids* 39(6), 1009-1023.

El-Adawy, M., Heikal, M. R., Aziz, A. R. A., Munir, S. and M. I. Siddiqui (2018a). Effect of Boost Pressure on the In-Cylinder Tumble-Motion of GDI Engine under Steady-State Conditions using Stereoscopic-PIV. *Journal of Applied Fluid Mechanics* 11(3), 733-742.

El-Adawy, M., Heikal, M., A Aziz, A., Adam, I., Ismael, M., Babiker, M., ... & Abidin, E. (2018 b). On the Application of Proper Orthogonal Decomposition (POD) for In-Cylinder Flow Analysis. *Energies* 11(9), 2261.

El-Adawy, M., M. R. Heikal, A. R. A. Aziz, M. I. Siddiqui and H. A. A. Wahhab (2017a). Experimental study on an IC engine in-cylinder flow using different steady-state flow benches. *Alexandria Engineering Journal*.

El-Adawy, M., M. R. Heikal, A. R. A. Aziz, M. I. Siddiqui and S. Munir (2017b). Characterization of the Inlet Port Flow under Steady-State Conditions Using PIV and POD. *Energies* 10(12), 1950.

Falfari, S., F. Brusiani and P. Pelloni (2014). 3D CFD analysis of the influence of some geometrical engine parameters on small PFI engine performances–the effects on the tumble motion and the mean turbulent intensity distribution. *Energy Procedia* 45, 701-710.

Fu, J., G. Zhu, F. Zhou, J. Liu, Y. Xia and S. Wang (2016). Experimental investigation on the influences of exhaust gas recirculation coupling with intake tumble on gasoline engine economy and emission performance. *Energy Conversion and Management* 127, 424-436.

Funk, C., V. Sick, D. L. Reuss and W. J. Dahm (2002). Turbulence properties of high and low swirl in-cylinder flows. *SAE technical paper* 2002(01), 2841

Heywood, J. B. (1988). Internal combustion engine fundamentals.

Huang, R. F., C. W. Huang, S. B. Chang, H. S. Yang, T. W. Lin and W. Y. Hsu (2005). Topological flow evolutions in cylinder of a motored engine during intake and compression strokes. *Journal of Fluids and Structures* 20(1), 105-127.

Kim, M., S. Lee and W. Kim (2006). Tumble flow measurements using three different methods and its effects on fuel economy and emissions. *In ASME 2006 Internal Combustion Engine Division Spring Technical Conference. American Society of Mechanical Engineers* 267-277

Korakianitis, T., A. M. Namasivayam and R. J. Crookes (2011). Natural-gas fueled spark-ignition (SI) and compression-ignition (CI) engine performance and emissions. *Progress in Energy and Combustion Science* 37(1), 89-112.

Krishna, A. S., Mallikarjuna, J. M. and D. Kumar (2016). Effect of engine parameters on in-cylinder flows in a two-stroke gasoline direct injection engine. *Applied Energy* 176, 282-294.

Lee, K., C. Bae and K. Kang (2007). The effects of tumble and swirl flows on flame propagation in a four-valve SI engine. *Applied Thermal Engineering* 27(11-12), 2122-2130.

Li, Y., H. Zhao, B. Leach, T. Ma and N. Ladommatos (2003). Optimisation of in-cylinder flow for fuel stratification in a three-valve twin-spark-plug SI engine. *SAE Technical Paper* 2003(01), 0635

Liu, D., T. Wang, M. Jia and G. Wang (2012). Cycle-to-cycle variation analysis of in-cylinder flow in a gasoline engine with variable valve lift. *Experiments in Fluids* 53(3), 585-602.

Millo, F., S. Luisi, F. Borean and A. Stroppiana (2014). Numerical and experimental investigation on combustion characteristics of a spark ignition engine with an early intake valve closing load control. *Fuel* 121, 298-310.

Müller, S. H. R., B. Böhm, M. Gleißner, R. Grzeszik, S. Arndt and A. Dreizler (2010). Flow field measurements in an optically accessible, direct-injection spray-guided internal combustion engine using high-speed PIV. *Experiments in Fluids* 48(2), 281-290.

Payri, F., J. Benajes, X. Margot and A. Gil (2004). CFD modeling of the in-cylinder flow in direct-injection Diesel engines. *Computers & Fluids* 33(8), 995-1021.

Reuss, D. L. (2000). Cyclic variability of large-scale turbulent structures in directed and undirected IC engine flows. *SAE Technical Paper* 2000(01), 0246

Reuss, D. L., R. J. Adrian, C. C. Landreth, D. T. French and T. D. Fansler (1989). Instantaneous planar measurements of velocity and large-scale vorticity and strain rate in an engine using particle-image velocimetry. *In International Congress and Exposition.*

Shuliang, L., L., Yufeng and L. Ming (2000). Prediction of tumble speed in the cylinder of the 4-valve spark ignition engines. *SAE Technical*

Paper 2000(1), 0247

Stansfield, P., G. Wigley, T. Justham, J. Catto and G. Pitcher (2007). PIV analysis of in-cylinder flow structures over a range of realistic engine speeds. *Experiments in Fluids* 43(1), 135-146.

Voisine, M., L. Thomas, J. Borée and P. Rey (2011). Spatio-temporal structure and cycle to cycle variations of an in-cylinder tumbling flow. *Experiments in Fluids* 50(5), 1393-1407

Wallner, T., S. A. Miers and S. McConnell (2008). A comparison of ethanol and butanol as oxygenates using a direct-injection, spark-ignition (DISI) engine. *In ASME 2008 Internal Combustion Engine Division Spring Technical Conference American Society of Mechanical Engineers* 129-139

Wang, T. Y., Z. J. Peng and G. D. Wang (2011). In-cylinder air motion characteristics with variable valve lift in a spark ignition engine. Part 1: swirl flow. *Proceedings of the Institution of Mechanical Engineers, Part D: Journal of Automobile Engineering* 225(4), 479-497.

Zhang, Z., H. Zhang, T. Wang and M. Jia (2014). Effects of tumble combined with EGR (exhaust gas recirculation) on the combustion and emissions in a spark ignition engine at part loads. *Energy* 65, 18-24.